Tracking vibrational energy on curved shell structures of variable thickness in the mid-to-high frequency limit - a ray-tracing approach

J J Crofts [1,2], **N Søndergaard** [2] **and D J Chappell** [1]
[1] Nottingham Trent University, School of Science and Technology,
Department of Physics and Mathematics, Nottingham, UK
e-mail: **jonathan.crofts@ntu.ac.uk**

[2] inuTech GmbH, 90429 Nürnberg, Germany

Abstract

Modelling the vibro-acoustic properties of mechanical built-up structures is a challenging task. Commonly employed techniques, such as finite element methods, are robust only in the low frequency regime. Recently, Discrete Flow Mapping has been forwarded as a cost efficient alternative method for mid- to high-frequency vibro-acoustic modelling. Discrete Flow Mapping employs local ray tracing approximations, providing a good model of the ray dynamics in homogeneous, isotropic flat plates or on curved shells in the geodesic high-frequency limit. However, in the mid-frequency case when the wavelength approaches the shell's local radius of curvature, the resulting ray dynamics depend on the curvature in a non-trivial way. In this work, we consider ray-tracing approaches for modelling vibrational energy transport in curved shells of variable thickness at mid-to-high frequencies. In particular, we analyse mid-frequency effects on the dispersion curves for curved shells of variable thickness, and identify novel reflection/transmission behaviour.

1 Introduction

Structure borne noise propagation in curved shells is, in general, characterised by directed wave energy transport. Ray tracing is well suited for capturing such directed propagation at mid-to-high frequencies, whereas popular statistical methods such as statistical energy analysis (SEA) often have problems capturing directed energy transport [1]. Ray tracing is used in a wide range of applications including in room acoustics, radar scattering and seismology [2] as well as in computer graphics [3]. However, ray based methods have not been widely adopted for structural engineering applications and this includes the application of interest for this study: modelling vibrational energy propagation on curved shells of variable thickness.

A methodology known as Dynamical Energy Analysis (DEA) has relatively recently been proposed for modelling vibrational energy propagation using ideas from ray tracing and dynamical systems [4]. Depending on the order of approximation of the wave energy density, DEA interpolates between SEA and full ray tracing. DEA has been implemented for straight line rays [5, 6] and their curved equivalent, geodesic rays [7]. However, for propagation below and in the vicinity of the ring frequency, geodesic ray tracing no longer suffices. Applying an Eikonal approximation to the thin shell wave equations of Donell leads to modified dispersion curves [8], from which a ray dynamics can be obtained. These dispersion curves depend explicitly on both the local radii of curvature and the shell thickness. Regions of high curvature may lead to backscattering of rays (and waves) near bends [9, 10]. Changes in shell the thickness on such a bend will also contribute to this backscattering, as well as giving rise to refraction in accordance with Snell's Law.

Motivated by implementing these features in a DEA treatment, and thus into a noise and vibration simulation tool, we investigate a ray tracing model on a configuration of two plates joined to a segment of a cylindrical

shell below the ring frequency. We model the variations in curvature and thickness using smooth interpolation functions; applications of such a model include castings such as a car shock tower, or smoothly curved shells in general. This smoothness also allows for a phase-plane analysis of the problem, providing insight to the underlying dynamical behaviour. The aim is to uncover quantitative laws of reflection and transmission across the curved ridge for use in DEA. The idea is that given an underlying radius of curvature associated with the connection between two DEA subsystems and a given mode type, frequency and incoming direction, one can use the laws of reflection and transmission from the underlying ray tracing model to determine the behaviour in the DEA model. The extension of this methodology to complex meshed structures would follow using the Discrete Flow Mapping (DFM) technique [7] . Changes in material thickness between two DEA subsystems (or two DFM elements) must be accounted for in the ray tracing model and the effect of these thickness variations on the ray dynamics will be the main focus of this study.

In the next section, we give a brief and general introduction into the governing shell theory. We will then describe our ray-tracing model for a cylindrical ridge of variable thickness in §3. The results of a corresponding numerical study are presented in §4, including a phase-plane analysis of the ray dynamics from which one can infer the underlying physics in terms of reflection, transmission and refraction. Finally, in §5 we conclude the study and suggest directions for future study.

2 Thin shell theory

The thin shell theory of Donell is one of the simplest and most widely adopted models [11]. In this theory, the moments and transverse forces are expressed by the displacement w of the middle surface as known from the theory of laterally loaded plates. The displacement vector of a point originally on the mid-surface of the shell is decomposed into tangential and normal components as $\mathbf{u} = [u^1\ u^2\ w]$.

For an isotropic shell of thickness h, Young's modulus E, density ρ and Poisson ratio ν, the shell equation for the normal displacement is given by [8]

$$\begin{aligned}\rho h \frac{\partial^2 w}{\partial t^2} &= -D_\alpha D_\beta \left(B(1-\nu) D^\alpha D^\beta w \right) - D_\alpha D^\alpha \left(B\nu D_\beta D^\beta w \right) \\ &\quad - C \left((1-\nu) d^\alpha_\beta \epsilon^\beta_\alpha + \nu d^\alpha_\alpha \epsilon^\beta_\beta \right),\end{aligned} \tag{1}$$

where

$$B = \frac{Eh^3}{12(1-\nu^2)} \quad \text{and} \quad C = \frac{Eh}{1-\nu^2} \tag{2}$$

are the bending and extensional stiffness, respectively. Note that these quantities are both spatially dependent due the the spatial dependence of the thickness h. All Greek alphabet indices take values from the set $\{1, 2\}$. The membrane strain is given by

$$\epsilon_{\alpha\beta} = \frac{1}{2} \left(D_\alpha u_\beta + D_\beta u_\alpha \right) + d_{\alpha\beta} w, \tag{3}$$

while the tangential displacements (u^1, u^2) in the directions (x^1, x^2), respectively, satisfy [8]

$$\rho h \frac{\partial^2 u^\alpha}{\partial t^2} = D_\beta \left(C \left((1-\nu) \epsilon^{\alpha\beta} + \nu \epsilon^\gamma_\gamma g^{\alpha\beta} \right) \right). \tag{4}$$

Here, $d_{\alpha\beta}$ denotes the covariant surface curvature tensor, $g_{\alpha\beta}$ the covariant metric tensor and D_α covariant differentiation with respect to the coordinate x^α. Note that contravariant and mixed forms of the above tensors are then obtained in the usual manner [12].

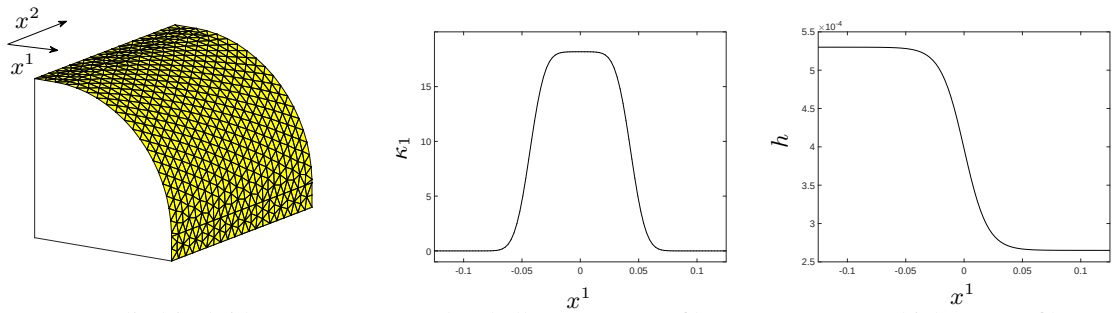

(a) Cylindrical ridge (b) Shell curvature profile (c) Thickness profile

Figure 1: Curvature and shell thickness profiles for the cylindrical ridge model introduced in §2.

2.1 Simplified model for a singly curved shell of variable thickness

In this Section we adopt the above shell theory of Donell to consider the case of a cylindrical ridge consisting of a cylindrical section with radius of curvature R coupled smoothly to two planar sections. We assume that the cylindrical ridge has principal curvature $\kappa_1(x^1)$ in the x^1 direction and zero curvature in the x^2 direction; see Fig. 1a. Note that in that case, the curvature tensor $d_{\alpha\beta} = 1$ if $\alpha = \beta = 1$ and is otherwise zero, whilst the metric tensor has components given by $g_{\alpha\beta} = 0$ if $\alpha \neq \beta$, $g_{11} = R^2$ and $g_{22} = 1$.

We assume that the principal curvature $\kappa_1(x^1)$ is of the form

$$\kappa_1(x^1) = \frac{f(x^1)}{f(0)}\kappa_{\text{cyl}}, \tag{5}$$

where κ_{cyl} denotes the maximum curvature of the cylindrical region, and f is an interpolation function given by

$$f(x^1) = \frac{1}{2}\left[\text{erf}\left(\frac{x^1 + x^*}{\Delta x}\right) - \text{erf}\left(\frac{x^1 - x^*}{\Delta x}\right)\right].$$

This choice of interpolation function f leads to a curvature profile that smoothly interpolates between zero (flat) and κ_{cyc} (cylindrical) across a small transition region of width Δx as shown in Fig. 1b. The centres of the transition regions are located on either side of the cylindrical ridge at $x^1 = \pm\, x^*$. The maximum curvature in the cylindrical region is denoted $\kappa_{\text{cyl}} = 1/R$.

In addition, we consider shells with variable thickness profiles of the form

$$h(x) = h_{\max}\left[1 - \frac{pe^{\beta x}}{1 + e^{\beta x}}\right] \tag{6}$$

where $h_{\max}$ denotes the maximum shell-thickness, $p \in (0, 1)$ controls the minimal shell-thickness, $ph_{\max}$, and β is a steepness parameter controlling the rate at which shell-thickness varies. This thickness profile is shown in Fig. 1c for $\beta = 100$ and $p = 0.5$. These are also the parameter values applied in our experiments, although similar results were found over a range of parameter values.

3 From waves to rays

A ray-tracing model is obtained from equations (1) and (4) by moving to the short wavelength asymptotics using the ansatz

$$\mathbf{u}(x, y, t) = \mathbf{u}^{(\epsilon)}(x^1, x^2, t)\exp\left(\mathrm{i}\epsilon^{-\lambda}\phi\left(x^1, x^2, \epsilon^{\mu}t\right)\right), \tag{7}$$

where ϕ is a phase function and ϵ is a small parameter. Defining the angular frequency $\omega = -\phi(x^1, x^2, \epsilon^{\mu}t)$ and the wavenumber vector $\mathbf{k}$ to have entries $k_\alpha = D_\alpha\phi(x^1, x^2, \epsilon^{\mu}t)$, one can study either bending or

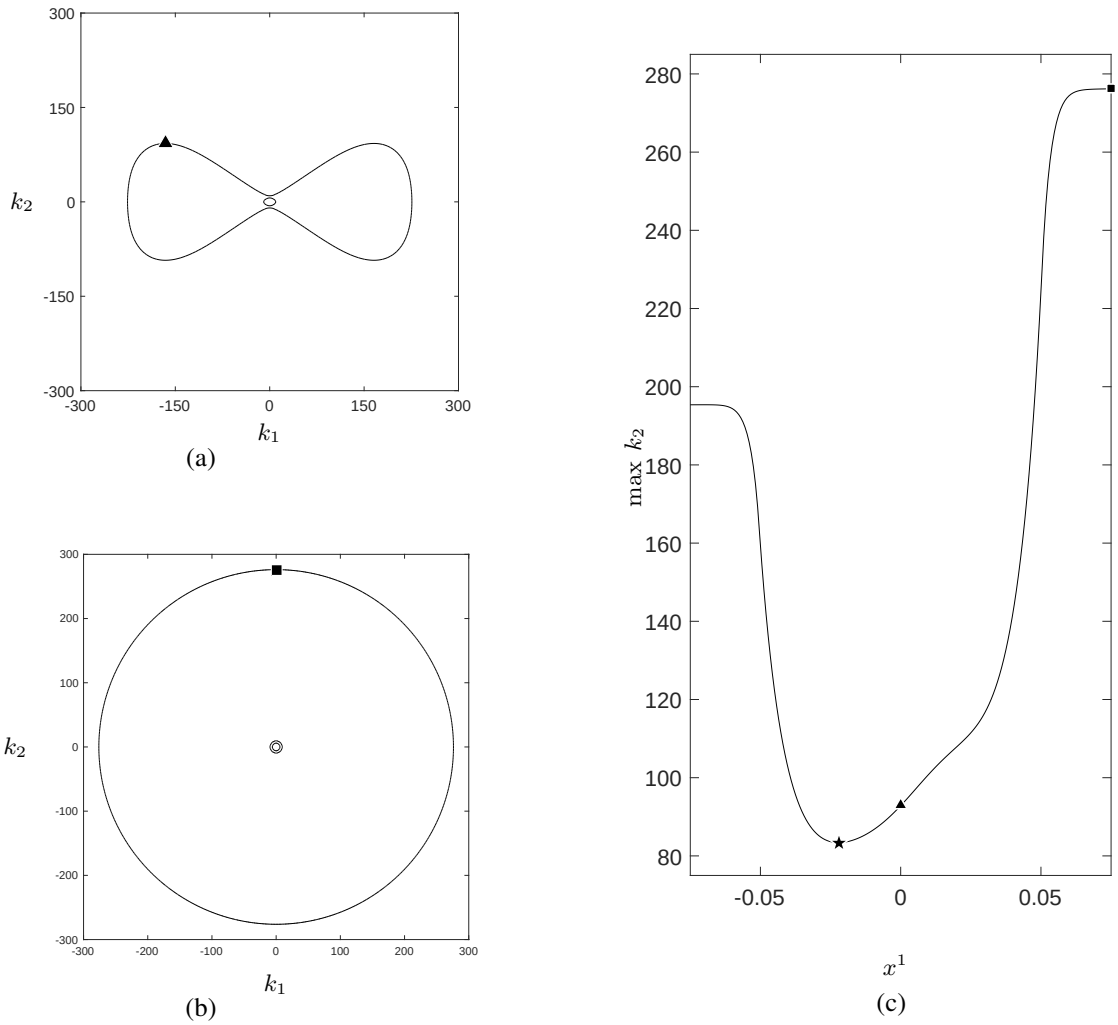

Figure 2: Plots (a) and (b) show respectively the dispersion relations for a cylinder and a flat plate. Plot (c) displays the maximum k_2 value of the dispersion relation as a function of x^1. The maximal values of the dispersion relations shown in plots (a) and (b) are highlighted, respectively, by triangular and square markers, as well as the global minima – which can be used to determine rules for transmission/reflection (see §4).

in-plane waves by selecting different choices of the parameters $\lambda \geq 0$ and $0 \leq \mu \leq \lambda$. Note that the prefactors of t vanish after applying the asymptotic scaling and setting $\lambda = \mu = 0$. Assuming that $k = |\mathbf{k}|$ is large in comparison to curvature, Pierce derived a general dispersion relation [11] that was later presented in a simplified form by Norris and Rebinsky [8]. This dispersion relation can be employed to generate a Hamiltonian formulation of the ray tracing model for a singly curved shell of variable thickness as described in the next section.

3.1 Ray tracing below the ring frequency

The ring frequency for the cylinder is defined relative to the extensional mode and corresponds to the frequency above which a longitudinal wave can traverse around the cylinder. Slightly above and around the ring frequency, approximate forms for the in-plane and bending modes are obtained using different scalings and eventually well beyond the ring frequency the dispersion relations reduce to those of a flat plate. Let us define the longitudinal wavenumber as $\Omega = \omega/c_L$, with c_L the longitudinal plate wave speed. Denoting the wavenumber at the ring frequency as $\Omega = \Omega_R$, we find that for the singly curved geometry under

consideration in this work we have $\Omega_R = \kappa_1$ where κ_1 is the principal curvature in the x^1 direction.

Below the ring frequency, the full dispersion relationship is usually considered. For the configuration in Figure 1a with zero curvature in the x^2-direction we obtain the following expression from [8] in physical coordinates:

$$\begin{aligned} H(x^1, k, \omega) = &\left(\Omega^2 - \frac{1}{2}k^2(1-\nu)\right)\left((\Omega^2 - k^2)\left(\Omega^2 - \frac{h(x^1)^2k^4}{12}\right)\right) \\ &+ (1-\nu^2)\left(\Omega^2\kappa_1(x^1)^2k_2^2 - \frac{1}{2}(1-\nu)\kappa_1(x^1)^2k_2^4\right). \end{aligned} \tag{8}$$

Note that here we have emphasised the x^1- dependence of both the shell thickness h and the principle curvature κ^1. Dispersion relations for a cylinder and flat plate are shown in figures 2a and 2b, respectively, for the parameter values given in Appendix A. Note that the outer part of the dispersion curve for the cylinder shown in Fig. 2a has also been observed experimentally [13].

For frequency domain problems with isotropic materials, such as those considered in this work, the Hamiltonian H defined in (8) gives rise to the following system of four ordinary differential equations (ODEs) that govern the ray dynamics on a singly curved shell:

$$\dot{x}^\alpha = \frac{\partial H}{\partial k_\alpha} \tag{9}$$

$$\dot{k}_\alpha = -\frac{\partial H}{\partial x^\alpha}. \tag{10}$$

Note that due to the translational invariance in the x^2-direction, it suffices to study the above system of ODEs in the (x^1, k_1) phase-plane only.

4 Numerical results

In this section we investigate the transmission/reflection behaviour of rays corresponding to an incident bending mode (see Figure 3). A range of incoming directions are used corresponding to a strip in the lower right corner of the figure. We find that rays transmit for sufficiently large values of $|k_1|$, whereas for smaller values of $|k_1|$ the rays reflect. As for the case of a shell with constant thickness studied in Refs. [9, 10], it is possible to determine a threshold value (k_1^*, k_2^*) such that for values of the tangential wavenumber k_2 below the threshold we have transmission and for k_2 above the threshold we have reflection. This leads to a simple transmission-reflection law of the form:

$$\text{Transmission probability}(k_2) = \begin{cases} 1 & \text{if } k_2 < k_2^* \\ 0 & \text{otherwise.} \end{cases} \tag{11}$$

The threshold value defined above can be shown to correspond to a hyperbolic fixed point, and in particular, the separatrices emanating from this point, which can be seen to divide the phase space into distinct transmission and reflection regions. To determine the location of the fixed point, it is convenient to consider the size of the dispersion curves as a function of x^1 (see Figure 2). In particular, note that the tangential wavenumber k_2 is constant along each trajectory as a consequence of Eq. (10), which gives that $\dot{k}_2 = 0$ due to translational invariance in x^2. Hence, transmission can only occur for values of k_2 that exist for all values of x^1. Note that this observation provides a practical means for computing the fixed point by considering the function, F say, that for each x^1 value returns the maximal k_2 value of the corresponding dispersion curve. The global minima of this function corresponds to the fixed point, that is

$$(x^{*1}, k_2^*) = (\operatorname{argmin} F, \min F). \tag{12}$$

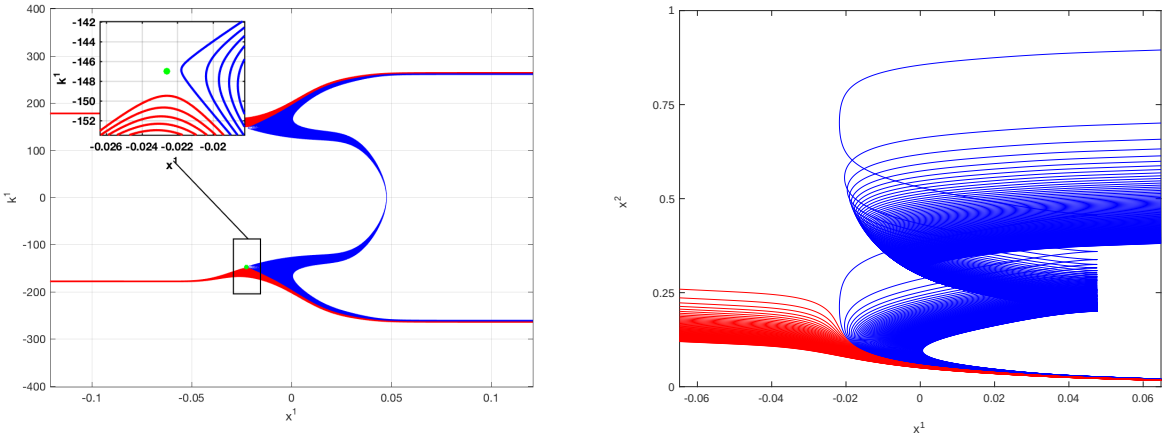

(a) (b)

Figure 3: Ray trajectories represented in (a) the (x^1, k_1) phase-plane and (b) the (x^1, x^2) plane. The close up in (a) shows the hyperbolic fixed point $(x^{*1}, k_1^*) \approx (-0.2275, -147)$ that determines transmission-reflection behaviour on the ridge for waves incoming from the right.

The above procedure was implemented (see Figure 2c) to determine the lower fixed point shown in Figure 3a and to obtain a numerical approximation of the corresponding threshold value for waves incoming from the right as $(k_1^*, k_2^*) = (-263.38, 83.39)$.

Compared to the constant thickness model considered in [9, 10], the main differences in the variable thickness case studied here relate to the loss of reflective symmetry of the (x^1, k_1) phase-plane about the line $x^1 = 0$. Note that for any transmitting trajectory, the change in the value of k_1 between the left and right sides of the ridge corresponds to a refraction according to Snell's Law. In the numerical experiment here, the thickness of the plate on the left is twice as thick as the plate on the right. This leads to a ratio of $\sqrt{2}$ between the bending wavenumbers on the right and the left. Figures 4a and 4b show this loss of symmetry and that the transmitted trajectories in Fig. 4b emerge on the right with an increase in the absolute value of the wavenumber k_1. From the above, it is straightforward to derive that this increase must obey

$$k_R^2 = 2k_L^2 + k_2^2, \tag{13}$$

where k_L corresponds to k_1 on the left-hand side and k_R corresponds to k_1 on the right; recall that k_2 is constant along the whole trajectory. We observe from our numerical results that this relation holds for the calculations shown in Fig. 4b. As a consequence of this, the wavenumber threshold also becomes dependent on whether the incoming ray approaches the ridge from the thicker plate on the left, or the thinner plate to the right. Here, the wavenumber threshold for incoming waves from the left (see Figure 4b) is given by $(k_1^*, k_2^*) = (176.66, 83.39)$, compared with $(k_1^*, k_2^*) = (-263.38, 83.39)$ for incoming waves from the right given above. Note that these threshold wavenumbers satisfy the relation (13) as expected.

5 Conclusions

We have performed ray tracing for a cylindrical ridge smoothly connected to two flat plates of differing thickness using Donell's shell theory. In particular, our calculations suggest the existence of a threshold incident wavenumber separating rays that exhibit reflective or transmissive behaviour. Importantly, in contrast to the constant shell thickness case [9, 10], the wavenumber threshold depends on whether the incident wave approaches the ridge from the thicker or the thinner plate and transmitted rays undergo refraction according to Snell's Law. These results suggest that relatively simple scattering laws can be deployed to model the propagation of structure-borne noise in shells of variable thickness, and ultimately to built-up structures

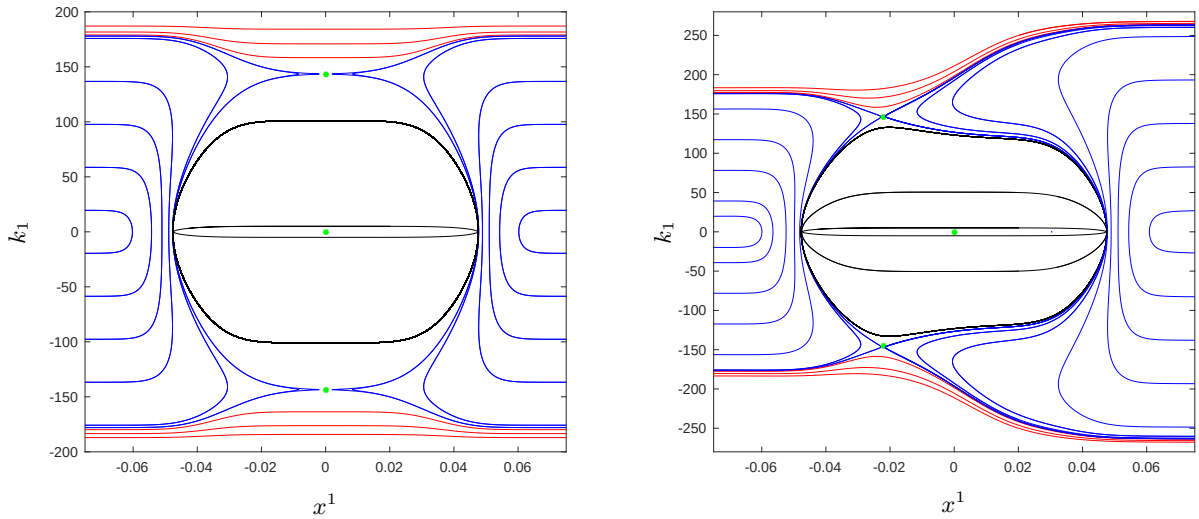

(a) (b)

Figure 4: Phase portraits for the cylindrical ridge model with (a) constant thickness as studied in [9, 10] (obtained by setting $p = 0$ in Equation (6)); and (b) variable thickness with $p = 0.5$.

containing thin shell components. Future work shall focus on extending the results here to multiply-curved shells, as well as incorporating the observed scattering laws into ray-based simulations of built-up structures using Dynamical Energy Analysis.

Acknowledgements

Support from the EU (FP7 IAPP grant 612237: MHiVec) is gratefully acknowledged. We also wish to thank Prof. Gregor Tanner for the stimulating discussions which motivated this study.

References

[1] R.S. Langley, *Wave motion and energy flow in cylindrical shells*, J. Sound Vib., 169(1), 29, 1994.

[2] H. Kuttruff, *Room Acoustics*, 4th edn. Spon, London (2000).

[3] J.T. Kayija, *The rendering equation, In Proc. SIGGRAPH 1986*: 143, DOI:10.1145/15922.15902 (1986).

[4] G. Tanner, *Dynamical energy analysis - Determining wave energy distributions in vibro-acoustical structures in the high-frequency regime*, J. Sound. Vib., **320**, 1023-1038 (2009).

[5] D.J. Chappell, S. Giani, G. Tanner, *Dynamical energy analysis for built-up acoustic systems at high frequencies*, JASA, 130(3), 1420, 2011.

[6] D.J. Chappell, G. Tanner, S. Giani, *Boundary element dynamical energy analysis: A versatile method for solving two or three dimensional wave problems in the high frequency limit*, J. Comp. Phys, 231, 6181, 2012.

[7] D.J. Chappell, G. Tanner, D. Lochel, N. Sondergaard, *Discrete flow mapping: transport of phase space densities on triangulated surfaces*, Proc. R. Soc. London, Ser. A, 469 (2013), 20130153.

[8] A.N. Norris, D.A. Rebinsky, *Membrane and Flexural Waves on Thin Shells*, J. Vib. Acoust., 116, 457, 1994.

[9] N. Søndergaard, D.J. Chappell, G. Tanner, *Tracking vibrational energy on curved shell structures in the mid-to-high frequency limit – a ray-tracing approach*, *Proceedings of Noise and Vibration – Emerging Technologies (NOVEM) 2015, Dubrovnik, Croatia, 2015*.

[10] N. Søndergaard, D.J. Chappell, *Ray and wave scattering in smoothly curved thin shell cylindrical ridges*, J. Sound. Vib., to appear.

[11] A.D. Pierce, *Waves on fluid-loaded inhomogeneous elastic shells of arbitrary shape*, Struct. Acoust. ASME, NCA-Vol. 12/AMD-Vol. 128, 195, 1991.

[12] W. Flügge, *Tensor Analysis and Continuum Mechanics*, Springer, Berlin, 1972.

[13] E.G. Williams, B.H.Houston, J.A. Bucaro, *Experimental investigation of the wave propagation on a point-driven, submerged capped cylinder using K-space analysis*, JASA, 87 (2), 513, 1990.

[14] D.A. Rebinsky, A.N. Norris, *Dispersion of Flexural Waves on Shells*, J. Vib. Acoust., 118, 526, 1996.

Appendix A Parameter values for the numerical studies

The computations throughout this work were done using the following parameter choices [13, 14]:

- $R = 55.0$ mm.
- $h_0 = 0.53$ mm.
- $x^* = 43.2$ mm.
- $\Delta x = 14.4$ mm.
- $E = 195$ GPa.
- $\rho = 7700\ \mathrm{kg/m^3}$.
- $\nu = 0.28$.
- $\omega = 9742\pi$ Rad/s.